

Generalized Model Predictive Direct Torque Control: Long Prediction Horizons and Minimization of Switching Losses

Tobias Geyer, *Member, IEEE*

Abstract—This paper presents a generalized Model Predictive Direct Torque Control scheme with an extended horizon, which is composed of multiple hinges (groups of switch transitions) linked by several extrapolation segments. The controller's performance is further enhanced by minimizing the switching losses in the inverter. Initial results suggest that with respect to state of the art Direct Torque Control, the switching losses are reduced by up to 60 %, while the Total Harmonic Distortion of the torque is at the same time improved by 20 %. These results are based on a medium-voltage three-phase Neutral Point Clamped inverter driving an induction machine.

Index Terms—Direct Torque Control, Model Predictive Control, Variable Speed Drive, Switching Losses, Power Electronics

I. INTRODUCTION

Three-phase electrical drives in the medium-voltage range with power ratings between one and several dozen megawatts are widely used in industries such as oil and gas, pulp and paper, mining and minerals, metals, power generation and marine, where they drive compressors, pumps, fans, blowers, conveyors, crushers and rolling mills, to name just a few. To achieve variable speed operation, an inverter with semiconductor switches is placed between the grid and the electrical machine, which is typically an induction motor.

Direct Torque Control (DTC) is ABB's method of choice for controlling three-phase electrical drives. Since its introduction in 1985 by Takahashi and Noguchi [1], DTC has quickly matured to an industrial standard for drive control [2]. The basic characteristic of DTC is that the inverter's switch positions are directly rather than indirectly set, thus refraining from using modulation techniques such as Pulse Width or Space Vector Modulation. In its generic form, the control objective is to keep both the motor's torque and the amplitude of the stator flux within given bounds. Using hysteresis controllers, the inverter is triggered to switch whenever these bounds are violated using a pre-designed look-up table. The main advantages of DTC are its superior torque performance with very short response times, its simple implementation and its inherent robustness. Significant effort has been spent in the past on improving the look-up table with the goal of reducing both the torque ripple and the switching frequency.

Recently, predictive control schemes and particularly Model Predictive Control (MPC) [3]–[5] have received considerable attention in the power electronics and drives community. Although MPC was originally developed for the process industry with its very long sampling intervals of minutes and more, the ever increasing computational power available nowadays and the possibility to solve off-line the online optimization problem [6] make MPC also applicable to fast processes with short sampling intervals such as power

electronics, where the sampling intervals are typically well below 100 μ s.

Even though DTC itself is widely interpreted as a predictive control strategy, it predicts only one step (one switch transition) ahead, and it lacks an internal model, a cost function and the notion of optimality, which are fundamental elements of an MPC scheme. Some of these elements are now present in the more recent approaches [7]–[13]. Yet, these schemes differ in several significant aspects from the control scheme proposed in this paper, for example by restricting the prediction horizon to one, by formulating a reference tracking problem, and by adding a modulator, to name a few. A more detailed literature study is available in [14] and [15].

With the aim of improving the performance of DTC by reducing the switching frequency whilst maintaining the very fast torque response, we started to work on MPC for power electronics in mid 2002. Specifically, the hysteresis bounds were inherited from standard DTC, whereas the DTC switching table was replaced by MPC. Starting with a closed-form Mixed-Integer Linear Optimization problem that was solved online [16], we subsequently pre-solved the optimization problem off-line and computed a look-up table [17]. An alternative open-form problem formulation that was also solved off-line reduced the controller complexity by an order of magnitude [18]. Model Predictive Direct Torque Control (MPDTC) [14], [15], which relies on a tailored open-form optimization problem solved online proved to be successful in the sense that its modest computational burden enabled ABB to implement it on its existing control platform. The successful test runs on ABB's ACS 6000 drive with power levels exceeding one MW [19], [20] can be considered as a milestone in the development of MPC for electrical drives.

In this paper, the previously proposed MPDTC algorithm is generalized thus allowing longer prediction horizons that include multiple hinges (groups of switch transitions) and extrapolation segments. The resulting prediction horizons are in the range of 50 to more than 100 time-steps. Moreover, similar to [21], the inverter losses are minimized rather than the switching frequency.

The paper is organized as follows. After describing the drive system in the next section, the control problem is stated in Section III. The generalized MPDTC scheme is detailed in Section IV, whilst its performance is benchmarked against standard DTC and the original MPDTC scheme in Section V. Section VI provides concluding remarks.

II. DRIVE SYSTEM

Throughout this paper, we will use normalized quantities. Extending this to the time scale t , one time unit corresponds to $1/\omega_b$ seconds, where ω_b is the base angular velocity.

T. Geyer is currently with the Department of Electrical and Computer Engineering, The University of Auckland, New Zealand, t.geyer@ieee.org

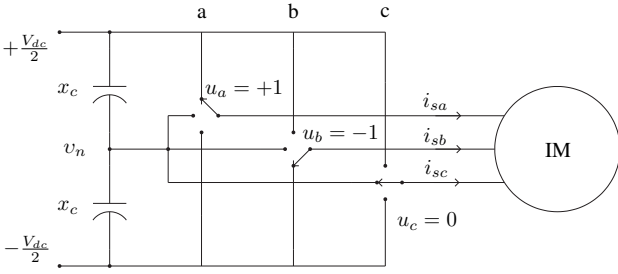


Fig. 1: Equivalent representation of a three-level Neutral Point Clamped (NPC) voltage source inverter driving an induction motor (IM)

A. The $\alpha\beta 0$ Reference Frame

All variables $\xi_{abc} = [\xi_a \ \xi_b \ \xi_c]^T$ in the three-phase system (abc) are transformed to $\xi_{\alpha\beta 0} = [\xi_\alpha \ \xi_\beta \ \xi_0]^T$ in the orthogonal $\alpha\beta 0$ stationary reference frame through

$$\xi_{\alpha\beta 0} = P \xi_{abc}. \quad (1)$$

Using the $\alpha\beta 0$ reference frame and aligning the α -axis with the a-axis, the following transformation matrix is obtained

$$P = \frac{2}{3} \begin{bmatrix} 1 & -\frac{1}{2} & -\frac{1}{2} \\ 0 & \frac{\sqrt{3}}{2} & -\frac{\sqrt{3}}{2} \\ \frac{1}{2} & \frac{1}{2} & \frac{1}{2} \end{bmatrix}. \quad (2)$$

B. Physical Model of the Drive System

The equivalent representation of a three-level Neutral Point Clamped (NPC) voltage source inverter driving an induction motor is shown in Fig. 1. In such a system, the dc-link is fed from the grid either by a (passive) diode front end or an (active) front end similar to the inverter. Here, the total dc-link voltage V_{dc} over the two dc-link capacitors x_c is assumed to be constant, while the neutral point potential v_n between the two capacitors is floating. Each phase leg can produce the three voltages $-\frac{V_{dc}}{2}, 0, \frac{V_{dc}}{2}$. Let the integer variables $u_a, u_b, u_c \in \{-1, 0, 1\}$ denote the switch positions in each phase leg – the so called phase states, where the values $-1, 0, 1$ correspond to the phase voltages $-\frac{V_{dc}}{2}, 0, \frac{V_{dc}}{2}$, respectively. Note that 27 different switch combinations exist. The actual voltage applied to the machine terminals is given by $v_{\alpha\beta 0} = 0.5V_{dc} P u_{abc}$ with $u_{abc} = [u_a \ u_b \ u_c]^T$.

As can be seen in Fig. 1, the neutral point potential v_n depends on the state of charge of the two dc-link capacitors and is only affected when current is drawn directly from it, i.e. when one of the switch positions is zero. This yields

$$\frac{dv_n}{dt} = -\frac{1}{2x_c} \left((1 - |u_a|)i_{sa} + (1 - |u_b|)i_{sb} + (1 - |u_c|)i_{sc} \right) \quad (3)$$

with the stator phase currents i_{sa}, i_{sb}, i_{sc} and one of the two symmetric capacitors x_c of the dc-link.

To describe the induction motor, a very accurate and detailed model is used. This model includes the saturation of the machine's magnetic material and the changes of the rotor resistance due to the skin effect. The detailed mathematical model is omitted here due to space limitations.

C. Constraints on the Switch Transitions

In the inverter considered here – due to the fact that only one di/dt snubber is available in the upper and the lower half, respectively – not all switch transitions are possible.

Polarity of the phase current	Switch transition	Switching losses
$i_{ph} > 0$	$0 \rightarrow 1$	$E_{on,1} + E_{rr,5}$
	$1 \rightarrow 0$	$E_{off,1}$
	$0 \rightarrow -1$	$E_{off,2} + E_{rr,5}$
	$-1 \rightarrow 0$	$E_{on,2} + E_{rr,3} + E_{rr,4}$
$i_{ph} < 0$	$0 \rightarrow 1$	$E_{off,3} + E_{rr,6}$
	$1 \rightarrow 0$	$E_{rr,1} + E_{rr,2} + E_{on,3}$
	$0 \rightarrow -1$	$E_{on,4} + E_{rr,6}$
	$-1 \rightarrow 0$	$E_{off,4}$

TABLE I: Switching losses in a 3-level phase leg

Specifically, each phase leg can switch only by at most one step, at most two phase legs can switch at the same time and if so, switching needs to occur in the opposite halves of the inverter. For example, from $[1 \ 1 \ 1]^T$, switching is only admissible to $[0 \ 1 \ 1]^T$, $[1 \ 0 \ 1]^T$ or $[1 \ 1 \ 0]^T$ (and not to any of the other 23 switch positions).

D. Switching Losses

The losses in the semiconductors can be divided into switching losses (arising when the devices is switched on or off) and conduction losses (due to the ohmic resistance). These losses depend on the applied voltage, the commutated current and the semiconductor characteristics. Considering Integrated Gate Commutated Thyristors (IGCT), with the GCT being the semiconductor switch, the switch-on and switch-off losses can be well approximated to be linear in the dc-link voltage and the phase current. Observing that in a NPC inverter, the voltage seen by each semiconductor is always half the total dc-link voltage leads to the GCT turn-on (energy) loss

$$E_{on} = e_{on} \frac{1}{2} V_{dc} i_{ph}, \quad (4)$$

where e_{on} is a coefficient and i_{ph} is the phase current. For the GCT turn-off losses, a corresponding equation results with the coefficient e_{off} . Typically, e_{off} is an order of magnitude larger than e_{on} .

For a diode, the switch-on losses are effectively zero. The turn-off losses, however, which are reverse recovery losses, are linear in the voltage, but nonlinear in the commutated phase current.

$$E_{rr} = e_{rr} \frac{1}{2} V_{dc} f_{rr}(i_{ph}), \quad (5)$$

where e_{rr} is the coefficient for the reverse recovery losses, and $f_{rr}(\cdot)$ is a nonlinear function between zero and one that is typically concave and saturating at one. Usually, the value of the coefficient e_{rr} lies in the interval between e_{on} and e_{off} .

Consider one three-level phase leg with the phase current i_{ph} and the three phase leg switch positions 1, 0 and -1. Then, by inspecting the phase leg topology, the switching losses per commutation can be derived. Since the commutation depends on the polarity of the phase current, the cases with positive and negative phase current need to be treated separately. Table I summarizes the switching losses, where the indices one to four refer to the GCT and freewheeling diodes, and the indices five and six refer to the NPC diodes.

Similar to the switching losses, the conduction losses also depend on the applied voltage and the phase current. The dc-link voltage is constant despite the neutral point fluctuations. The phase current is the sum of the current ripple and the fundamental component, which in turn depends only on the

operating point given by the torque and the speed, but not on the switching pattern. Since the ripple is small compared to the fundamental current (typically in the range of 10% for a 3-level inverter), the conduction losses can be considered to be independent from the switching pattern. Hence, they are not addressed in the objective function.

III. CONTROL PROBLEM

The DTC control objectives are to keep the three output variables, namely the electromagnetic torque, the length (or magnitude) of the stator flux and the neutral point potential, within given (hysteresis) bounds. In MPDTC, these objectives are inherited from DTC. In addition, we aim at minimizing the inverter losses. An indirect way of doing that is to minimize the (short-term) average switching frequency [15], [16]. Here, we will directly target the switching losses so as to further improve the performance (lower the losses).

Apart from that, the produced torque should be smooth and have a little harmonic content only. A measure for this is the Total Harmonic Distortion (THD) of the electromagnetic torque. Obviously, the minimization of the torque and/or the current THD on the one side, and the switching losses on the other side is a conflicting objective.

IV. MODEL PREDICTIVE DIRECT TORQUE CONTROL

A. Model Predictive Control

In MPC [3], the current control input is obtained by solving at each sampling instant a constrained optimal control problem based on the predictions provided by an internal model of the controlled process. The optimal control problem is formulated over a finite or infinite horizon using the current state of the plant as initial state. The underlying optimization procedure yields an optimal control sequence that minimizes a given objective function. Only the first control input of this sequence is applied in accordance with the so called receding horizon policy. At the next sampling instant, the control sequence is recomputed over a shifted horizon, thus providing feedback. Hence, MPC combines (open-loop) constrained optimal control with a receding horizon policy.

B. Internal Controller Model

Hereafter, we derive a discrete-time model of the drive that is suitable to serve as an internal prediction model for MPDTC. The model's purpose is to predict the trajectories of the electromagnetic torque, the stator flux and the inverter neutral point potential over several sampling intervals in an open-loop fashion.

The squirrel-cage induction motor is modelled in the $\alpha\beta$ reference frame using the α and β -components of the stator and the rotor flux linkages per second as state vector $\psi = [\psi_{s\alpha} \ \psi_{s\beta} \ \psi_{r\alpha} \ \psi_{r\beta}]^T$. As the time-constant of the rotor speed dynamic exceeds the length of the prediction interval by several orders of magnitude, the rotor speed dynamics are neglected and the rotor's rotational speed ω_r is assumed to remain constant within the prediction horizon. This allows us to treat the speed as a model parameter rather than as a state. The other model parameters are the base angular velocity ω_b , the stator and rotor resistances r_s and r_r , and the stator, rotor and mutual reactances x_{ls} , x_{lr} and x_m , respectively.

Recall that we are using normalized quantities and a normalized time-axis. Referring the rotor quantities to the stator circuit, the continuous-time state equation [22]

$$\frac{d\psi}{dt} = \begin{bmatrix} -r_s \frac{x_{rr}}{D} & 0 & r_s \frac{x_m}{D} & 0 \\ 0 & -r_s \frac{x_{rr}}{D} & 0 & r_s \frac{x_m}{D} \\ r_r \frac{x_m}{D} & 0 & -r_r \frac{x_{ss}}{D} & -\omega_r \\ 0 & r_r \frac{x_m}{D} & \omega_r & -r_r \frac{x_{ss}}{D} \end{bmatrix} \psi + v \quad (6)$$

results, with $x_{ss} = x_{ls} + x_m$, $x_{rr} = x_{lr} + x_m$, $D = x_{ss}x_{rr} - x_m^2$ and $v = [v_\alpha \ v_\beta \ 0 \ 0]^T$. The electromagnetic torque is given by

$$T_e = \frac{x_m}{D} (\psi_{s\beta} \psi_{r\alpha} - \psi_{s\alpha} \psi_{r\beta}) \quad (7)$$

and the length of the stator flux vector is

$$\Psi_s = \sqrt{\psi_{s\alpha}^2 + \psi_{s\beta}^2}. \quad (8)$$

We define the overall state vector of the drive as $x = [\psi_{s\alpha} \ \psi_{s\beta} \ \psi_{r\alpha} \ \psi_{r\beta} \ v_n]^T$, the switch positions as the input vector $u = u_{abc} = [u_a \ u_b \ u_c]^T \in \{-1, 0, 1\}^3$, and the electromagnetic torque, the length of the stator flux and the neutral point potential as the output vector $y = [T_e \ \Psi_s \ v_n]^T$.

Combining the motor model (6)–(8) with the inverter model (3), taking advantage of the fact that the α and β -components of the stator current $i_{s,\alpha\beta 0}$ are linear combinations of the stator and rotor flux components (see e.g. [22] for details), i.e.

$$i_{s,\alpha\beta 0} = \frac{1}{D} [x_{rr} \psi_{s\alpha} - x_m \psi_{r\alpha} \quad x_{rr} \psi_{s\beta} - x_m \psi_{r\beta} \quad 0]^T,$$

and using the Euler formula, a discrete-time model of the drive can be derived. As in standard DTC, a sampling interval of $T_s = 25 \mu\text{s}$ is used. The resulting state equation is bilinear in the input variable due to (3), and the output equation is quadratic. The discrete-time model is omitted here due to space limitations, but it can be found in [14] or [15].

C. Generalized MPDTC Algorithm

The generalized MPDTC algorithm is based on a Last In First Out stack model, commonly used in computer science. Starting at the current time-step k , the algorithm iteratively explores the tree of feasible switching sequences forward in time. At each intermediate step, all switching sequences must yield output trajectories that are either *feasible*, or *pointing in the proper direction*. We refer to these switching sequences as *candidate* sequences. Feasibility means that the output variable lies within its corresponding bounds; pointing in the proper direction refers to the case in which an output variable is not necessarily feasible, but the degree of the bounds' violation decreases at every time-step within the switching horizon. The above conditions need to hold *componentwise*, i.e. for all three output variables¹.

The traversing through the tree is controlled by the so called *switching horizon* composed of the elements 'S' and 'E', which stand for 'switch' and 'extrapolate' (or more generally 'extend'), respectively. The switching horizon, with its upper bound on the number of switch transitions and extension steps, can be considered as an alternative to a (fixed) prediction horizon in time. Note that for MPDTC,

¹As an example, consider the case where the torque is feasible, the stator flux points in the proper direction and the neutral point potential is feasible.

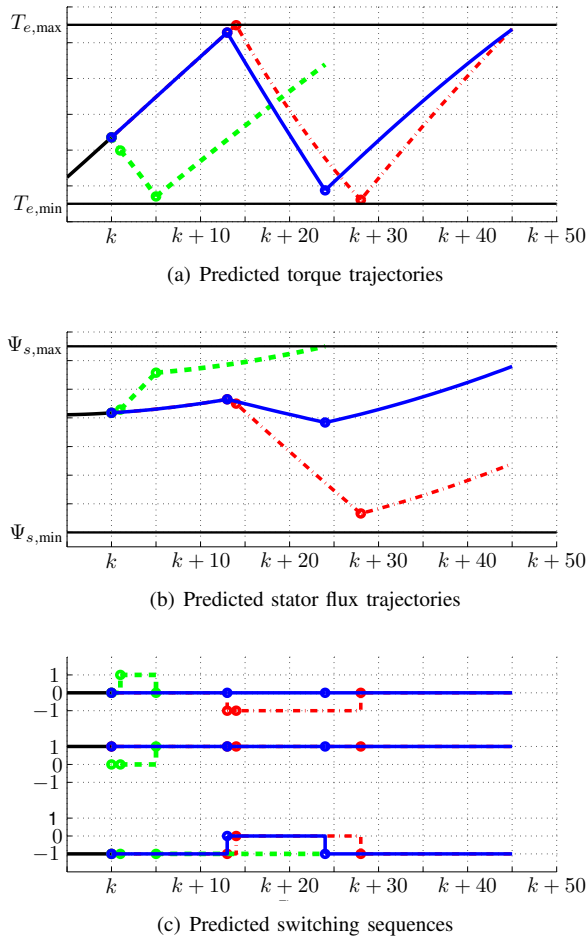


Fig. 2: Three candidate switching sequences for the switching horizon 'eSSESE' with the associated torque and stator flux trajectories between their respective upper and lower bounds. The time-axis is given by the sampling instants with the sampling interval $T_s = 25 \mu s$.

the resulting prediction horizon is of variable length in time. As an example for a switching horizon, consider 'SSESE', which stands for switching at time-steps k and $k + 1$ and subsequently extending the trajectories until one or more output trajectory ceases to be feasible and/or pointing in the proper direction. Assume this happens at time-step $k + \ell$ thus triggering the third switching event that is followed by another extension step. We use the task 'e' to add an optional extension leg to the switching horizon. Using 'eSSESE' as an example, three candidate switching sequences are depicted in Fig. 2 along with their output trajectories.

At time-step k , the generalized MPDTC algorithm computes $u(k)$ according to the following procedure.

- 1) Initialize the root node with the current state vector $x(k)$, the last switch position $u(k - 1)$ and the switching horizon. Push the root node onto the stack.
- 2a) Take the top node with a non-empty switching horizon from the stack.
- 2b) Read out the first element. For 'S', branch on all feasible switch transitions according to Section II-C. For 'E', extend the trajectories either by extrapolation as detailed in [14] or by using the internal controller model of Section IV-B.

Induction Motor			
Voltage	3300 V	r_s	0.0108 p.u.
Current	356 A	r_r	0.0091 p.u.
Real power	1.587 MW	x_{ls}	0.1493 p.u.
Apparent power	2.035 MVA	x_{lr}	0.1104 p.u.
Frequency	50 Hz	x_m	2.3489 p.u.
Rotational speed	596 rpm		
Inverter			
Dc-link voltage	4294 V	V_{dc}	1.5937 p.u.
		x_c	11.769 p.u.

TABLE II: Rated values (left) and parameters (right) of the drive

- 2c) Keep only the switching sequences that are candidates.
- 2d) Push these sequences onto the stack.
- 2e) Stop if there are no more nodes with non-empty switching horizons. The result of this are the predicted (candidate) switching sequences $U^i(k) = [u^i(k), \dots, u^i(k + n_i - 1)]$ over the variable-length horizons n_i , where $i \in \mathcal{I}$ and \mathcal{I} is an index set.
- 3) Compute for each (candidate) sequence $i \in \mathcal{I}$ the associated cost. If the switching frequency is to be minimized, consider $c_i = s_i/n_i$, which approximates the average switching frequency, where $s_i = \sum_{\ell=k}^{k+n_i-1} \|u_i(\ell) - u_i(\ell - 1)\|_1$ is the total number of switch transitions in the switching sequence $U^i(k)$, and n_i is the corresponding sequence length. Conversely, if the losses are targeted, the cost function $c_i = E_i/n_i$ is used, where E_i are the switching losses according to Section II-D. Note that, to compute the losses, the phase currents need to be derived, which are linear combinations of the flux components, thus making this a simple operation.
- 4) Choose the switching sequence $U^* = U^i(k)$ with the minimal cost, where $i = \arg \min_{i \in \mathcal{I}} c_i$.
- 5) Apply (only) the first switch position $u(k) = u^*$ of this sequence and execute the above procedure at the next time-step $k + 1$.

The main differences to the MPDTC algorithm reported previously in [14], [15] are that, unlike before, a candidate switching sequence must yield output trajectories that are feasible or pointing in the proper direction at *every* time step. This ensures that the bounds are respected at all times during steady-state operation. Secondly, the algorithm runs iteratively, i.e. instead of first enumerating the switching sequences and then computing the associated output trajectories, the switching sequences are built step-wise by branching on the feasible switch transitions. One advantage of this is that it is straightforward to extend the switching horizon by considering multiple switchings and multiple extrapolation steps. Moreover, branch and bound techniques can be added to reduce the computational burden.

V. PERFORMANCE EVALUATION

This section benchmarks the generalized MPDTC scheme with respect to standard DTC. The comparison is made based on the ACS 6000 drive system [23] with a 3.3 kV and 50 Hz squirrel-cage induction machine rated at 2.5 MVA. The detailed parameters can be found in Table II. For this comparison, a very accurate and detailed Matlab/Simulink model of the drive is used, which was provided by ABB to ensure as realistic a simulation set-up as possible. This model includes a state estimator for the motor fluxes, and an outer (speed) control loop that adjusts the torque reference

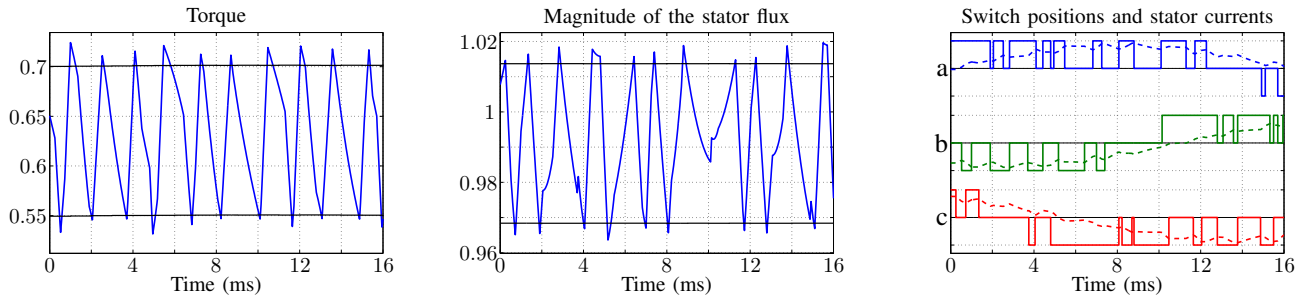


Fig. 3: Standard DTC: Steady-state operation at 60% speed and 60% torque. All quantities are given in p.u.

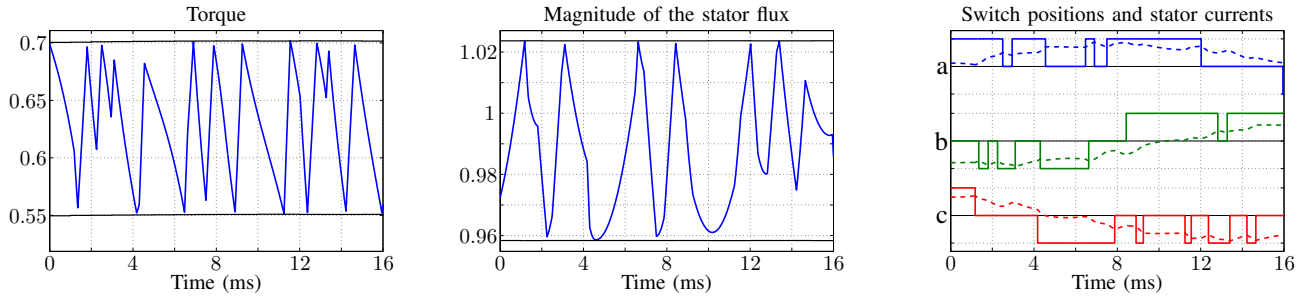


Fig. 4: MPDTC with the switching horizon 'eSSESSE' and a penalty on the switching frequency: Steady-state operation at 60% speed and 60% torque. All quantities are given in p.u.

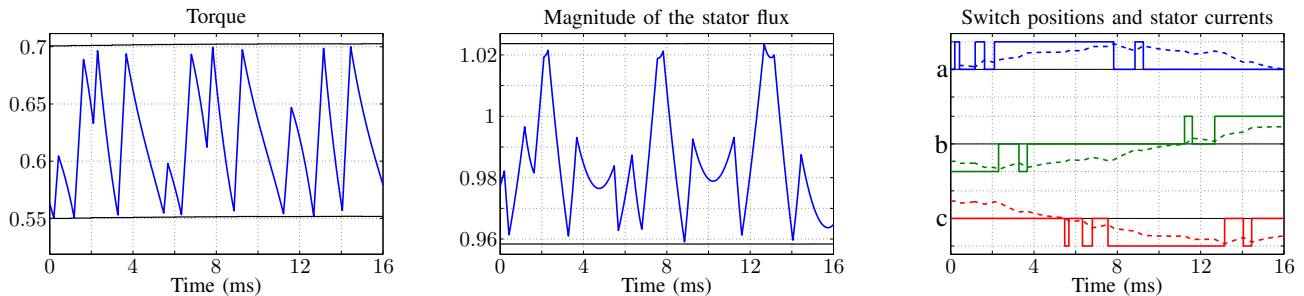


Fig. 5: MPDTC with the switching horizon 'eSSESSE' and a penalty on the switching losses: Steady-state operation at 60% speed and 60% torque. All quantities are given in p.u.

and the (time-varying) bounds on the torque accordingly. The induction motor model includes the saturation of the machine's magnetic material and the changes of the rotor resistance due to the skin effect. For MPDTC, the look-up table with the standard DTC strategy is replaced by a function that runs the generalized MPDTC algorithm at each sampling-instant. The significance of such simulations is underlined by the very close match between previous simulations and experimental results using the same model. The simulation results in [15] predicted the experimental results in [20] accurately to within a few percent.

A. Transient Performance

For torque steps, standard DTC has a very fast dynamic response, which is typically a few ms. In MPDTC, the rapid dynamic torque control is preserved, while the bounds imposed on the torque, stator flux and neutral point potential are slightly better respected by MPDTC (than DTC). The interested reader is referred to [14] and [15] for a detailed comparison based on step responses.

B. Steady-State Performance

Figs. 3-5 compare the steady state behavior of DTC and MPDTC penalizing the switching frequency and the losses, respectively, at 60% speed with a 60% torque setpoint. The same torque bounds are used for both control schemes, while for MPDTC the flux bounds are widened by ± 0.01 p.u. to account for DTC's violations of the flux bounds. For the neutral point potential the bounds are chosen so as to reflect the behavior of the standard DTC control scheme, thus ensuring that the comparison is meaningful. The figures show the torque and the stator flux magnitude in p.u. together with their respective bounds. The figures showing the neutral point potential, which is kept well within its bounds, are omitted here. The switch positions u_a, u_b, u_c of the three phase legs are plotted along with the respective phase currents i_{sa}, i_{sb}, i_{sc} . These three figures show one half period of the fundamental current waveform.

As can be seen in Fig. 3, standard DTC tends to switch when the phase currents are high and when the effect on the torque and flux is thus large. The torque, flux and neutral point potential are considered independently from each

Control scheme	Horizon	Minimization of	$T_{e,THD}$ [%]	f_{sw} [%]	P_{loss} [%]
Standard DTC	–	–	100	100	100
MPDTC	$N = 1$	f_{sw}	80.4	71.2	72.6
MPDTC	$N = 2$	f_{sw}	88.5	59.1	61.0
MPDTC	eSSE	f_{sw}	81.2	70.4	67.5
MPDTC	eSSESSE	f_{sw}	79.7	56.8	56.8
MPDTC	eSSESSE	f_{sw}	78.7	54.9	54.5
MPDTC	eSSE	P_{loss}	82.3	70.4	52.5
MPDTC	eSSESSE	P_{loss}	81.2	68.5	59.0
MPDTC	eSSESSE	P_{loss}	81.0	57.2	39.6

TABLE III: Comparison of standard DTC with MPDTC with various horizons and penalties. The comparison is done in terms of the torque THD $T_{e,THD}$, the switching frequency f_{sw} and the switching losses P_{loss} using standard DTC as the baseline. The operating point is at 60% speed and 60% torque.

other. In contrast to that, MPDTC considers all three output variables simultaneously in a Multiple Input Multiple Output (MIMO) control approach. As a result, c.f. Fig. 4, less switch transitions are required (particularly for the stator flux) thus reducing the switching frequency and also the switching losses. Yet, as in DTC, most of the switch transitions occur when the current is high. Penalizing the switching losses rather than the switching frequency, as shown in Fig. 5, centers 50% of the switch transitions around the phase currents' zero crossing, while the other 50% is centered around the current peak. Each of these groups of switching events covers 30 degrees of the fundamental. Taking into account that in a three-phase system the phases are shifted by 120 degrees, continuous switching is provided to keep the torque, flux and neutral point potential under control, while reducing the switching losses to a minimum.

Based on simulations run over 1 s, Table III compares various MPDTC schemes to DTC in terms of the torque THD, the switching frequency and the switching losses. These simulations refer to 60% speed with a 60% torque setpoint. As can be seen, with respect to DTC, MPDTC with the switching horizon 'eSSE' penalizing the switching frequency reduces the switching losses by 32%, while the switching frequency is reduced by 30%. As mentioned earlier, this algorithm is very similar to MPDTC with $N = 2$ as reported in [14], [15]. Penalizing the switching losses instead maintains the switching frequency improvement, whilst the switching losses are reduced by another 15%. Doubling the length of the horizon from 'eSSE' to 'eSSESSE' cuts down the losses by another 13%. At the same time, the torque THD is slightly reduced as the switching horizon is increased.

VI. CONCLUSIONS

At the chosen operating point, as indicated by Table III, the generalized MPDTC scheme with the long switching horizon 'eSSESSE' is expected to reduce the switching losses by 60%, while reducing the switching frequency by 43% when compared to DTC. At the same time, the torque THD is lowered by 19%, thus reducing both the inverter and the machine losses at the same time. This result can be used either to increase the current rating of the inverter, or to further reduce the torque THD (by narrowing the torque bounds and increasing the inverter losses). Currently, efforts are made to reduce the control scheme's computational complexity to make it suitable for an implementation.

ACKNOWLEDGMENTS

This work was supported by ABB Switzerland Ltd. The author would like to thank Georgios Papafotiou of ABB Corporate Research, Baden-Dättwil, Switzerland, and Christian Stulz of ABB ATDD, Turgi, Switzerland, for their advice.

REFERENCES

- [1] I. Takahashi and T. Noguchi. A new quick response and high efficiency control strategy for the induction motor. *IEEE Trans. Ind. Applicat.*, 22(2):820–827, Sep./Oct. 1986.
- [2] G. S. Buja and M. P. Kazmierkowski. Direct torque control of PWM inverter-fed AC motors – a survey. *IEEE Trans. Ind. Electron.*, 51(4):744–757, Aug. 2004.
- [3] C. E. Garcia, D. M. Prett, and M. Morari. Model predictive control: Theory and practice – a survey. *Automatica*, 25(3):335–348, Mar. 1989.
- [4] J.M. Maciejowski. *Predictive Control*. Prentice Hall, 2002.
- [5] S. J. Qin and T. A. Badgwell. A survey of industrial model predictive control technology. *Control Engineering Practice*, 11(7):733–764, Jul. 2003.
- [6] A. Bemporad, M. Morari, V. Dua, and E. N. Pistikopoulos. The explicit linear quadratic regulator for constrained systems. *Automatica*, 38(1):3–20, Jan. 2002.
- [7] R. Kennel, A. Linder, and M. Linke. Generalized predictive control (GPC) – ready for use in drive applications? In *Proc. IEEE Power Electron. Specialists Conf.*, volume 4, pages 1839–1844, Vancouver, Canada, 2001.
- [8] G. Escobar, A. M. Stanković, E. Galvan, J. M. Carrasco, and R. Ortega. A family of switching control strategies for the reduction of torque ripple in DTC. *IEEE Trans. Contr. Syst. Technol.*, 11(6):933–939, Sep. 2003.
- [9] J. Rodríguez, J. Pontt, C. Silva, P. Cortes, U. Amman, and S. Rees. Predictive direct torque control of an induction machine. In *Proc. IEEE Power Electron. and Motion Control Conf.*, Riga, Latvia, 2004.
- [10] J. M. Retif, X. Lin-Shi, A. M. Llor, and F. Morand. New hybrid direct-torque control for a winding rotor synchronous machine. In *Proc. IEEE Power Electron. Specialists Conf.*, volume 1, pages 1438–1442, Aachen, Germany, Jun. 2004.
- [11] A. Linder and R. Kennel. Model predictive control for electrical drives. In *Proc. IEEE Power Electron. Specialists Conf.*, pages 1793–1799, Recife, Brasil, 2005.
- [12] A. Linder and R. Kennel. Direct model predictive control – a new direct predictive control strategy for electrical drives. In *Proc. European Conf. on Power Electron. and Applicat.*, Dresden, Germany, Sep. 2005.
- [13] R. Vargas, P. Cortés, U. Ammann, J. Rodríguez, and J. Pontt. Predictive control of a three-phase neutral-point-clamped inverter. *IEEE Trans. Ind. Electron.*, 54(5):2697–2705, Oct. 2007.
- [14] T. Geyer. *Low Complexity Model Predictive Control in Power Electronics and Power Systems*. PhD thesis, Automatic Control Laboratory ETH Zurich, 2005.
- [15] T. Geyer, G. Papafotiou, and M. Morari. Model predictive direct torque control - part I: Concept, algorithm and analysis. *IEEE Trans. Ind. Electron.*, 56(6):1894–1905, Jun. 2009.
- [16] G. Papafotiou, T. Geyer, and M. Morari. Optimal direct torque control of three-phase symmetric induction motors. In *Proc. IEEE Conf. on Decision and Control*, Atlantis, Bahamas, Dec. 2004.
- [17] G. Papafotiou, T. Geyer, and M. Morari. A hybrid model predictive control approach to the direct torque control problem of induction motors (invited paper). *Int. J. of Robust Nonlinear Control*, 17(17):1572–1589, Nov. 2007.
- [18] T. Geyer and G. Papafotiou. Direct torque control for induction motor drives: A model predictive control approach based on feasibility. In M. Morari and L. Thiele, editors, *Hybrid Systems: Computation and Control*, volume 3414 of *LNCS*, pages 274–290. Springer, Mar. 2005.
- [19] J. Kley, G. Papafotiou, K. Papadopoulos, P. Bohren, and M. Morari. Performance evaluation of model predictive direct torque control. pages 4737–4744, Jun. 2008.
- [20] G. Papafotiou, J. Kley, K. G. Papadopoulos, P. Bohren, and M. Morari. Model predictive direct torque control - part II: Implementation and experimental evaluation. *IEEE Trans. Ind. Electron.*, 56(6):1906–1915, Jun. 2009.
- [21] S. Mastellone, G. Papafotiou, and E. Liakos. Model predictive direct torque control for MV drives with LC filters. In *Proc. European Power Electron. Conf.*, Barcelona, Spain, Sep. 2009.
- [22] P. C. Krause. *Analysis of Electric Machinery*. McGraw-Hill, NY, 1986.
- [23] ABB Asea Brown Boveri Ltd. Product webpage of ACS 6000. online document. www.abb.com/motors&drives.